Detection of Instrument Gain Problems Based on Body-Wave Polarization: Application to the Hi-Net Array

by Sunyoung Park and Miaki Ishii

ABSTRACT

Monitoring and assessing instrument performance and response are crucial to various seismological analyses that utilize the seismic signal recorded by the instrument. One of the important components of the instrument response is the gain or the amplification factor that determines the amplitude of the recorded wave arrival. We introduce a new method to detect problems in the gain of three-component seismographs by examining the body-wave polarization. Anomalous gain of a certain component causes *P*- and *S*-wave polarization to be distinct from expected values, allowing one to identify the issue in the instrument. The method is applied to the High-Sensitivity Seismograph Network (Hi-net) stations between 2004 and 2016, and 305 out of 790 stations are identified to have issues at various time periods. The detections are confirmed by comparison with the Hi-net daily calibration pulses. Utilization of teleseismic body-wave polarization information is an effective way to detect instrument gain problems without physically examining the instrument, which is particularly advantageous for instruments such as borehole or ocean-bottom sensors that cannot be accessed easily.

Electronic Supplement: Table with complete list of stations that are detected with gain issues in this study, and figures describing cases where the gain issues are identified by calibration pulse data.

INTRODUCTION

Seismic recordings provide invaluable data for understanding a wide range of subject matters such as Earth's structure and earthquake processes. Therefore, it is important to monitor the performance of seismic instruments and maintain them to a high standard by identifying issues. The user should also examine the seismic data and ensure their quality, because using problematic data may bias results and lead to wrong interpretations.

One of the important factors in data quality is the gain (also referred to as amplification factor) of instruments. If a research involves the absolute amplitude such as comparison of the amplitude measurements from different stations, or combination of more than one component recorded at a station, any unknown issues in the gain of the instruments or relative gain between different components will bias the analysis. Such analyses include estimation of earthquake magnitude (e.g., Veith and Clawson, 1972; Kanamori, 1977; Bullen and Bolt, 1985) and absolute ground motions (e.g., Boore and Joyner, 1982; Campbell, 1985; Douglas, 2001). Structural studies using more than two components of a seismograph such as analyses based on receiver function (e.g., Langston, 1979), Rayleigh-wave particle motion (e.g., Boore and Toksöz, 1969), and shear-wave splitting (e.g., Ando *et al.*, 1983; Silver and Chan, 1991) are also affected by instrument gain.

There are various mechanical, electrical, and observation-based methods to estimate the gain of an instrument. Mechanical approaches include using a reference sensor with a known response installed next to the sensor to be tested and comparing the recordings (e.g., Pavlis and Vernon, 1994), or imposing a step-function-type motion to the sensor and examining the recorded signal (Bormann, 2012). It is difficult, however, to evaluate any change in the instrument response due to transportation to the field. Applying a known signal such as a step-function like displacement, for example, of 1 mm, to a sensor and examining the recorded output is a straightforward method to assess the instrument response, but has the same issue with transportation. Moreover, it is not trivial to impose the input displacement that is accurate without any tilt (Havskov and Alguacil, 2004). Electrical methods use a calibration pulse to monitor the instrument responses (MacWilliams and Sloane, 1976; Berger *et al.*, 1979; MacArthur, 1985). These methods generate electronic current within the instrument instead of a mechanical input, and thus do not require physical access to the instrument. The calibration can be performed as frequently as necessary, usually daily. However, the calibration pulses can obscure and distort important signals such as seismic-wave arrivals, which has been the main reason that many seismic instruments do not adopt the daily calibrations. Moreover, the electrical methods cannot detect problems that

doi: 10.1785/0220180252

are related to the conversion between the mechanical input and the current (e.g., Wielandt, 2002; Havskov and Alguacil, 2004). On the other hand, examining observed signals can identify problems between the mechanical input and the final recordings. Ekström *et al.* (2006) used long-period (> 50 s) waves to detect gain problems in long-period instruments by scrutinizing the misfit between the actual recordings and the synthetic waveforms generated based on inverted centroid moment tensor solutions. For the very-long-period Global Seismic Network stations, normal-mode data from 2004 Sumatra earthquake and Earth's tide data have been utilized for the instrument calibration (Davis *et al.*, 2005; Davis and Berger, 2007).

In this article, we introduce an approach based on the teleseismic body-wave polarization that is computationally efficient and can be applied remotely and frequently for inspecting short-period or broadband instrument gain. The term polarization is used in this article to refer to the particle motion rather than the incident-wave direction. By examining the particle motion using the three-component recordings, one can identify components with anomalous amplification. The method is advantageous in that it does not require an artificial signal that can interfere with seismic-wave arrivals or a direct access to the instrument, and thus is suitable for difficult-to-access instruments such as borehole and ocean-bottom sensors. Moreover, it can monitor the instrument and identify gain problems in real time, allowing the station operators to report and fix the issue. To demonstrate the potential of the method, we apply the new technique to the High-Sensitivity Seismograph Network in Japan (Hi-net; Okada *et al.*, 2004) and compare the identified gain issues with instrument calibration pulses. A list of stations with time periods of gain problems is provided.

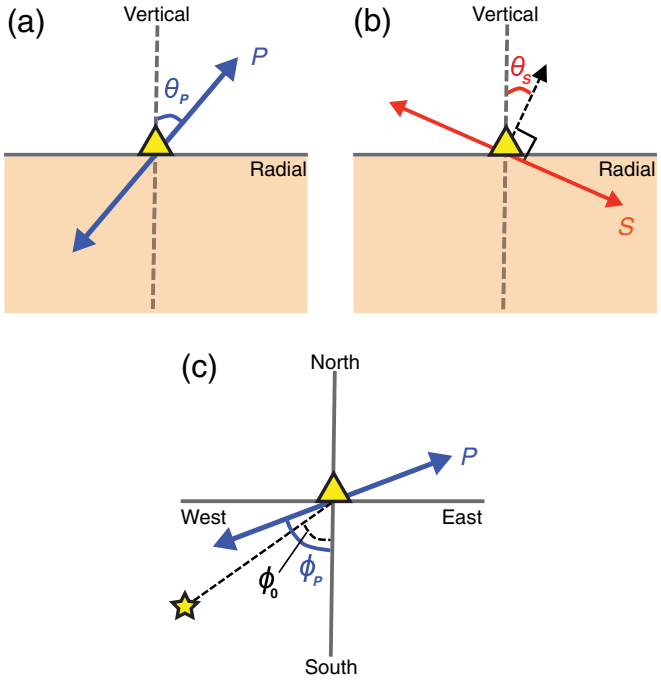

▲ **Figure 1.** Geometries of the observed particle motions in the vertical-radial plane for (a) *P* and (b) *S* waves, and (c) horizontal plane for *P* wave at a station (triangle). The particle motion or polarization directions are shown by arrows for *P* (blue) and *S* (red) waves. The angle θ_P corresponds to the apparent incident angle measured from the vertical (dashed line) for the *P* wave. The angle θ_S is defined similarly for *S* wave, except that it corresponds to the direction perpendicular to the particle motion. The angles ϕ_P and ϕ_0 are acute angles measured with respect to north-south direction for *P* wave and the back azimuth with respect to the earthquake (star), respectively.

METHOD

The particle motions of the teleseismic *P* and *S* waves arriving at a station depend on the geometry between the earthquake and the station, and the local near-surface wavespeed structure (Park and Ishii, 2018). The apparent incident direction for teleseismic *P* wave is usually between 10° and 30° from the vertical, and that for the *S* wave is between 10° and 40° from the horizontal direction. Although the azimuthal direction of *S*-wave motion depends on source mechanisms and can be complicated due to anisotropy (e.g., Silver and Chan, 1991), those for *P* waves align close to the back azimuth. Thus, the body-wave arrivals have finite vertical and horizontal angles that can be predicted based on the station-earthquake geometry and local structure, allowing one to examine the deviations from the expected values and identify issues in the relative gain of a three-component instrument.

We first measure the polarization directions of teleseismic *P* and *S* waves (Fig. 1) using the principal component analysis (Pearson, 1901) in the time domain (Park and Ishii, 2018). In addition to obtaining the apparent incident angles θ_P and θ_S for *P* and *S* waves, respectively, in the vertical-radial plane, the azimuthal angle of the *P* wave is obtained using the first principal component of the complete 3D data. The apparent *S*-wave incident angles are defined as the direction perpendicular to the particle motion. The azimuthal angles can take any angle from 0° to 360° depending on the station-earthquake geometry. Since the main focus of the analysis is to determine the amplitude ratio between components, i.e., how north-south or east-west the particle motion is, back azimuth of 90°, for example, is equivalent to 270°. Hence, the *P* azimuthal angles are converted to acute angles ϕ_P, measured from the north-south direction (Fig. 1c); for example, back azimuth of 350° becomes ϕ_P of 10°. Predicted back-azimuthal direction from station and earthquake geometry is also converted into acute angle ϕ_0 from the north-south direction. For each station, the three measured angles θ_P, θ_S, and ϕ_P, and the predicted azimuthal angle ϕ_0 are analyzed using multiple teleseismic earthquakes (Park and Ishii, 2018).

The angles are effective in detecting if one of the three components has anomalously low or high amplification factor relative to the other components. For example, if the vertical component has a considerably low gain, both *P* and *S* particle

motions will be dominantly recorded in horizontal components, resulting in θ_P close to 90° and θ_S close to 0°. On the contrary, if the vertical component has unusually high gain compared with the horizontal components, the P and S vertical angles θ_P and θ_S will become close to 0° and 90°, respectively. Similarly, for the two horizontal components, if the north-south component has anomalously low or high gain compared with the east-west component, the horizontal angle ϕ_P will be close to 90° or 0°.

Horizontal angle ϕ_P can theoretically be 0° or 90° without any gain problem if the station-earthquake geometry results in back azimuth of 0°, 90°, 180°, or 270°. Thus, for detecting gain problems, one needs to compare ϕ_P with ϕ_0. For the vertical angles, however, theoretical P and S particle motions are nearly perpendicular to each other, and cannot reproduce the effect of anomalous gain: P and S waves with horizontal motions at the same time, that is, θ_P of 90° and θ_S of 0°, or both with vertical motions, that is, θ_P of 0° and θ_S of 90°. Even in rare circumstances of extremely low near-surface wavespeeds underneath the station, θ_P and θ_S become near 0° at the same time, that is, vertical P and horizontal S, rather than one becoming 0° and the other 90° (Park and Ishii, 2018). Therefore, it is not necessary to compare θ_P and θ_S to their theoretical values.

Detection of the instrument problem is performed in two steps. The first step examines the consistency of the angles over time. Given that anomalous angles can arise from other factors such as noise in the data, we seek observations of unusual measurements that are persistent within a time window of length τ. For the jth time window centered at t_j, we take the median of the measurements within the window, that is, from $t_j - 0.5\tau$ to $t_j + 0.5\tau$, and denote them as $\bar{\theta}_P^j$, $\bar{\theta}_S^j$, and $\bar{\phi}_P^j$ (Fig. 2). We also examine the median of the absolute difference between the measured and predicted P-horizontal angles within the time window, that is, $\overline{|\phi_P - \phi_0|}^j$. The median values are checked to ensure they satisfy the following four criteria:

I. $\bar{\theta}_P^j > 90 - \Delta_\theta$ and $\bar{\theta}_S^j < \Delta_\theta$,
II. $\bar{\theta}_P^j < \Delta_\theta$ and $\bar{\theta}_S^j > 90 - \Delta_\theta$,
III. $\bar{\phi}_P^j > 90 - \Delta_\phi$ and $\overline{|\phi_P - \phi_0|}^j > \Delta_0$,
IV. $\bar{\phi}_P^j < \Delta_\phi$ and $\overline{|\phi_P - \phi_0|}^j > \Delta_0$,

in which Δ_θ and Δ_ϕ are small threshold angles for determining if the measured angles are close to vertical or horizontal and north-south or east-west directions, respectively, and Δ_0 is a threshold value to determine if measurements deviate significantly from the predicted angles. The criteria (I) and (II) indicate that the vertical sensor has significantly higher and lower gain, respectively, with respect to the horizontal sensors. The criteria (III) and (IV) indicate that the gain of the north-south sensor is too small and large, respectively, compared with the east-west sensor. The median values are more suitable than the averages because they are not strongly biased by the outliers. This first step allows the detection of time periods with gain problems that are longer than $\tau/2$, assuming the measurements are evenly distributed in time. The exact limit of the detectable duration can vary, however, due to the uneven spacing of the data resulting from nonuniform occurrence of teleseismic earthquakes. To enhance the detectability, τ should be selected to be the shortest duration that still includes more than a few measurements at any time t_j.

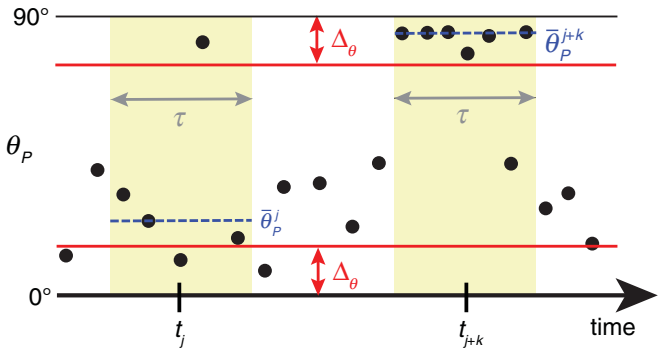

▲ **Figure 2.** Schematics of the first step of the detection process for P vertical angles θ_P (black circles) using moving time windows (yellow shades). At the jth timestep t_j, the time window of length τ is examined to calculate the median angle $\bar{\theta}_P^j$. The angle $\bar{\theta}_P^j$ is between the threshold values Δ_θ and $(90° - \Delta_\theta)$, and thus, the time window does not satisfy either criterion (I) or (II). For the $(j + k)$th time window, however, the angle $\bar{\theta}_P^{j+k}$ meets the first part of criterion (I).

The second step is to perform a cluster analysis (e.g., Anderberg, 1973; Jain and Dubes, 1988) to identify additional anomalous data that were not detected in the first step, for example, those with a short time span or less extreme values of angles. It is applied to the data that did not satisfy any of the four criteria in the previous step. Data from the ith earthquake are organized into a vector composed of four elements: t_i, θ_P^i, θ_S^i, and ϕ_P^i. The distance between vectors associated with different earthquakes is defined as the Euclidean distance where each of the four elements is normalized by its variance, that is, standardized. The distances are used to construct the agglomerative hierarchical cluster tree and to form clusters such that the average distances between clusters are larger than a cutoff value (e.g., Jain and Dubes, 1988). Clusters other than the largest are considered anomalous, except for clusters composed of a single vector from a single event, because it may be an outlier due to noise. For the same reason, clusters with minimum time separation between vectors longer than τ are not considered. Given the anomalous clusters, we examine data between the earliest and the latest times associated with the clusters. Any time window where the majority of the data are included in the clusters becomes our detected problematic time window. For example, a cluster of two anomalous data vectors would not be considered if the two are separated by more than τ or by more than two normal data vectors in between.

DATA

The new method for detecting the instrument response issue is applied to the Hi-net (Okada *et al.*, 2004) consisting of nearly 800 short-period three-component borehole instruments (Fig. 3a). The network provides daily calibration pulses for

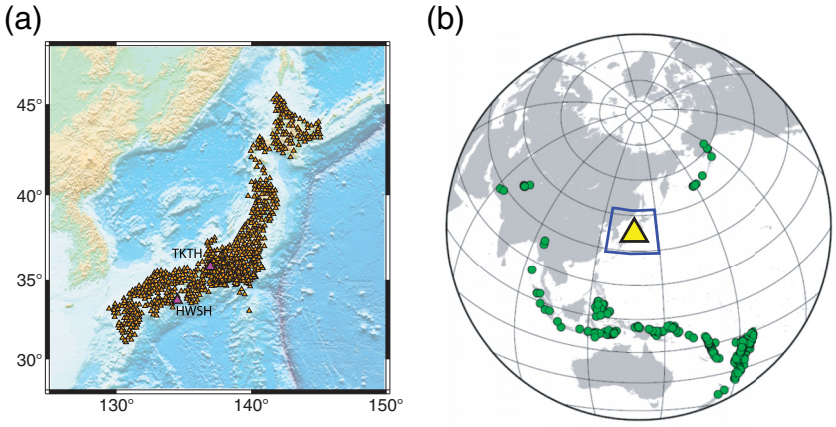

▲ **Figure 3.** (a) Distribution of the High-Sensitivity Seismograph Network (Hi-net) stations (orange triangles) plotted on a topography map based on ETOPO2 (National Geophysical Data Center, 2006). Stations TKTH and HWSH are marked with magenta triangles. (b) Distribution of the intermediate and deep events (green circles) at teleseismic distances with respect to the Hi-net (yellow triangle). The blue box represents the corresponding area shown in (a).

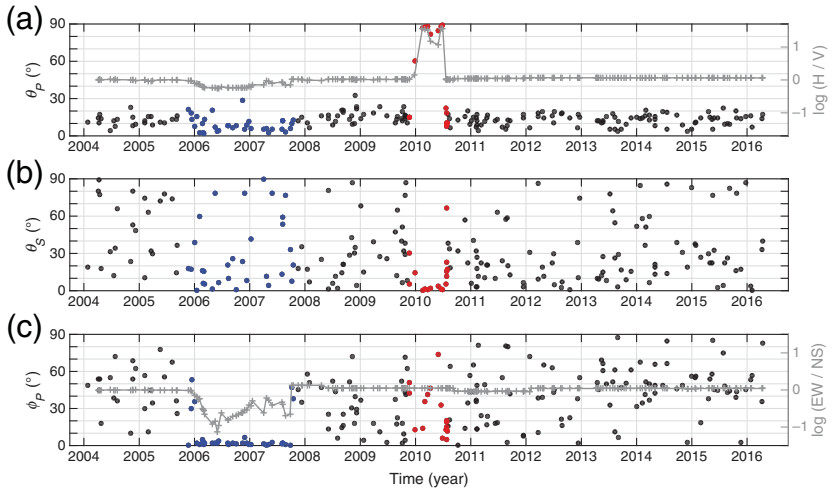

▲ **Figure 4.** Measured angles (circles) corresponding to (a) θ_P, (b) θ_S, and (c) ϕ_P at station TKTH. The data are shown as a function of time from 2004 to April 2016 and each circle corresponds to a teleseismic earthquake. Red and blue circles are those identified to have an instrument issue in the vertical and horizontal components, respectively, in the first step, while black circles belong to time periods without instrument issues. Gray lines with plus signs are amplitude ratio (a) between horizontal and vertical and (c) between the two horizontal components obtained using the Hi-net calibration peaks. The vertical axes labels on the right side denote vertical (V), east-west (EW), north-south (NS), and the average of the two horizontal (H) amplitudes. The amplitude ratios are plotted in log scales.

station maintenance (Obara *et al.*, 2005), and thus, is ideal for validating our technique by comparing the results with the calibration data. The National Research Institute for Earth Science and Disaster Resilience provides Hi-net waveform data, station misorientation information, and a "channels table" file that includes sensor gain information (see Data and Resources). The data are corrected for any known misorientation or gain issues.

We use earthquakes deeper than 60 km with $M_w > 6$ that occurred between 2004 January and 2016 April at the 30°–90° teleseismic distance range (Fig. 3b). The shallow events are excluded to ensure that the depth phases do not arrive close to the direct phase, which would contaminate the apparent incident-angle measurements. Regional earthquakes are not considered because triplicated phases due to the upper-mantle discontinuities and Moho complicate the particle motion. These selection criteria result in 234 earthquakes based on the U.S. Geological Survey National Earthquake Information Center catalog (see Data and Resources).

We discard data with signal-to-noise ratio (SNR) less than 2, calculated using all three components. The signal and noise windows are defined to be 5 s from the *P* and *S* onsets and to be between 10 and 5 s before the onset, respectively. The 5-s time windows have been demonstrated to be optimal in capturing the main arrivals and providing robust polarization measurements (Park and Ishii, 2018). The data are not filtered and the onset is automatically picked based on the continuous wavelet transform algorithm (Bogiatzis and Ishii, 2015).

For each station, measurements of θ_P, θ_S, and ϕ_P are collected (Figs. 4 and 5). Generally, θ_P ranges from near vertical to about 30° as expected for teleseismic arrivals, where the variation in the angle is mainly caused by different earthquake distances and noise in the data (Park and Ishii, 2018). The *S* apparent incident angle θ_S is also under 40° for the most robust measurements. However, the θ_S measurements have larger scatter than θ_P due to less clear *S* arrivals than the *P* arrivals. Additionally, for *S* waves, high SNR does not guarantee a good-quality *SV* signal, because the *S* signal window consists not only of the *SV* wave but also of *P*-coda and *SH* arrivals. The horizontal *P* angle ϕ_P is nearly evenly distributed from north-south to east-west directions, reflecting the azimuthal coverage of the earthquakes used in the analysis (Figs. 4 and 5).

RESULTS AND DISCUSSIONS

For each Hi-net station, the two-step procedure is performed. We tested using different values for the time window τ, thresholds Δ_θ, Δ_ϕ, and Δ_0, and the cutoff distance for the cluster

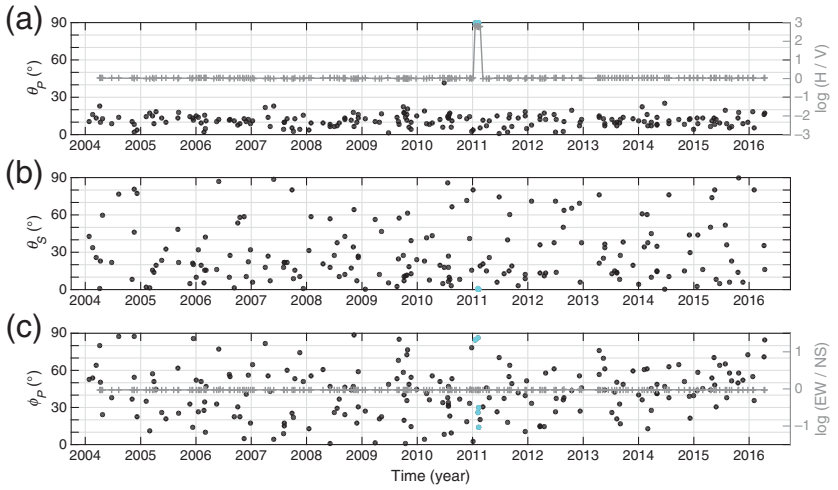

▲ **Figure 5.** Same as Figure 4, except for station HWSH and the cyan circles represent the identified instrument issues in the second step through cluster analysis. No black circle occurs within the time associated with the cyan circles.

analysis. For the time window τ, half a year is found to be optimal to include enough angle measurements to detect the persistent instrument issue while providing time resolution. In terms of the thresholds Δ_θ and Δ_ϕ, we find 10° and 5°, respectively, work well. Given that the available horizontal-angle measurements are only about half the number of vertical measurements and are more scattered, the smaller threshold, that is, stricter criterion, is necessary to ensure robust detection. The value considered for Δ_0 is 35°, larger than Δ_θ or Δ_ϕ, because the measured horizontal angles ϕ_P may deviate significantly from the predicted angles ϕ_0 due to anisotropic structure. We find the cutoff distance of 5 for the cluster analysis to be reasonable in detecting data that are distinct from the majority.

Performing the first step of the analysis detects issues at various time periods for 291 out of 790 Hi-net stations (Ⓔ Table S1, available in the electronic supplement to this article). For example, station TKTH has issues with its vertical component from the end of 2009 to mid-2010 (Fig. 4). The anomalous measurements correspond to criterion (I), indicating that the gain of the vertical component is more than an order of magnitude smaller compared with the horizontal components during this time period. Some measurements at the ends of the problematic time range, for example, at the end of 2009 and mid-2010, also satisfy criterion (I) even though their values are not anomalous. It is because the algorithm considers all measurements within the time window τ as potentially anomalous if any of the criteria (I)–(IV) is met. These measurements near the edges may not be anomalous, but we take a conservative approach to include and report them so that the remaining data are free of instrument problems for analyses such as the investigation of the near-surface wavespeeds (Park and Ishii, 2018). The θ_P of 60° at the start of 2010 represents a transition from normal to the low gain of the vertical component.

In addition to anomalies detected using the vertical angles, the station exhibits problems on the horizontal components from late 2005 to late 2007. During the time period, ϕ_P is close to zero, corresponding to the criterion (IV), indicating that the east-west component has amplification factor that is about 30 times smaller compared with the north-south component. This is also supported by θ_P being lower than the average, that is, the arrivals appear more vertical, caused by the total horizontal amplitude being smaller than it should be. Similar to the vertical-component detections, measurements without issues at both ends of the problematic time period are included due to duration τ.

The detected gain problems can be compared with the daily calibration pulses of the Hi-net instrument. We compute the two relative amplitudes, that is, between the vertical and the average horizontal and between the two horizontal components, and compare the ratios with the measured apparent incidence angles as a function of time (Fig. 4a,c). The issues detected with criteria (I) and (IV) for the station TKTH correspond to the time periods of the low vertical to horizontal and the low east-west to north-south amplitude ratios, respectively.

Among the 291 stations with problems identified in the first step, 81, 163, 89, and 65 correspond to the criteria (I)–(IV), respectively, indicating that there are more issues on the vertical component (relative to horizontal) than between the two horizontal components. Fifty-nine stations, including the station TKTH, exhibit issues on more than one component. For five stations, ASGH, HASH, NMTH, ODWH, and YSTH, the entire time periods are identified with issues, and 22 additional stations exhibit gain problems on more than half of their operation time (Ⓔ Table S1).

The cluster analysis in the second step detects anomalous time periods for 28 stations (Ⓔ Table S1). Among the 28 stations, 14 stations have measurements identified only in the second step. Station HWSH is one of the 14 stations where the detected measurements span for only about two months in early 2011, which is too short to be detected in the first step (Fig. 5). It is possible to shorten the τ in the first step to about two months, which may allow the detection of the same time window. Nevertheless, it is not ideal because the window is so short that it often includes up to a few measurements that are not sufficient for examining the persistence of the anomalous values. This detection using the cluster analysis is also confirmed by vertical amplification that is more than 300 times lower than other time periods based on the calibration pulses.

In general, our detections are compatible with the calibration data. Our method, similar to other empirical approaches (Davis *et al.*, 2005; Ekström *et al.*, 2006; Davis and Berger, 2007), identifies anomalous apparent gain, which can arise for various reasons; the actual cause of the problem needs to be investigated separately. The gain problems detected by

both our method and the calibration pulses can be attributed to factors such as issues with coils or conversion between force and electric voltage, a decentered mass, and a dead channel (e.g., Townsend, 2014).

We also find cases where the calibration pulse data show anomalies that are not detected in our analysis (Ⓔ Fig. S1). These cases occur either when the change in the relative amplitude is too subtle to be identified, or when there are issues in the process of converting the electric voltage to the force rather than an issue in the mechanical gain. The latter can be related to problems in test coils, where the calibration voltage is applied, which are distinct from signal coils (Ueno *et al.*, 2015). On the other hand, there are detections that do not appear as anomalies based on the calibration pulses. For example, the station SSWH has a long-term issue in the relative gain between the horizontal components that is not manifested in the calibration data (Ⓔ Fig. S2). Such cases suggest that there are issues in the ground coupling for the identified component.

After the two-step analysis, there are 305 stations with gain issues (Ⓔ Table S1). This is about 39% of the Hi-net stations, and overall, 6% of the entire measurements made at Hi-net have been detected as anomalous. For the 305 stations, this corresponds to about 15% of the measurements, or about 2-yr duration on average. In terms of occurrence times of instrument problems, it is similar to that of earthquakes used in the analysis, suggesting that there is no particular time window associated with issues at many stations. The amplitudes of detected gain issues are about a factor of 10 on average, and range from 2–2000.

CONCLUSIONS

We present a new technique to detect instrument issue using three-component seismograms based on teleseismic body-wave polarization. By examining the anomalous polarization angles of *P* and *S* waves, problems in the instrument gain between components are identified. The method is composed of two steps: (1) identifying time windows with problematic measurements and (2) finding additional anomalous measurements using cluster analysis.

The technique is applied to data from the Hi-net array, composed of 790 stations over 12 yrs. Issues are found for 291 stations from the first step of the procedure. The second step detects 14 additional stations, mostly associated with short-term instrument problems. The detected gain issues are verified by comparing with the Hi-net calibration pulse amplitude, demonstrating the efficacy of our detection method. A small fraction of our detections do not have corresponding counterparts in the calibration data, suggesting these problems arise from poor ground coupling.

The detection method introduced in this article is effective and efficient in computation, useful for both station operators and data users in identifying the instrument issues. This is valuable because most instruments do not perform the electrical calibration, and is especially valuable for instruments that are hard to access, such as ocean-bottom seismometers. Depending on the intended use of the results, one can control how conservative the detection need be by tuning parameters such as the durations of time windows, thresholds, and whether or not to classify the measurements near the ends of a detected time window as problematic. For example, larger thresholds may allow the method to detect smaller gain anomalies. Improving the data coverage in azimuth and incident angles or combining with surface-wave data can also help detect more subtle gain issues or misorientations in three-component seismograms.

DATA AND RESOURCES

The Hi-net waveform data, station misorientation information and "channels table" files are obtained from National Research Institute for Earth Science and Disaster Resilience (NIED) at http://www.hinet.bosai.go.jp (last accessed May 2018). The earthquake database was searched using the National Earthquake Information Center (NEIC) catalog at https://earthquake.usgs.gov (last accessed April 2016). Figure 3 was made using the Generic Mapping Tools v.5.1.1 (www.soest.hawaii.edu/gmt, last accessed January 2018; Wessel and Smith, 1991). ◪

ACKNOWLEDGMENTS

The authors thank Editor-in-Chief Zhigang Peng and the three anonymous reviewers for the helpful comments to improve the article. The authors also thank National Research Institute for Earth Science and Disaster Prevention in Japan for providing the data. This work is funded by National Science Foundation (NSF) Grant EAR-1735960. S. P. is supported by the Samsung Scholarship.

REFERENCES

Anderberg, M. R. (1973). *Cluster Analysis for Applications (No. OAS-TR-73-9)*, Office of the Assistant for Study Support Kirtland AFB N MEX, New York, New York.

Ando, M., Y. Ishikawa, and F. Yamazaki (1983). Shear wave polarization anisotropy in the upper mantle beneath Honshu, Japan, *J. Geophys. Res.* **88,** 5850–5864.

Berger, J., D. C. Agnew, R. L. Parker, and W. E. Farrell (1979). Seismic system calibration: 2. Cross-spectral calibration using random binary signals, *Bull. Seismol. Soc. Am.* **69,** 271–288.

Bogiatzis, P., and M. Ishii (2015). Continuous wavelet decomposition algorithms for automatic detection of compressional- and shear-wave arrival times, *Bull. Seismol. Soc. Am.* **105,** 1628–1641, doi: 10.1785/0120140267.

Boore, D. M., and W. B. Joyner (1982). The empirical prediction of ground motion, *Bull. Seismol. Soc. Am.* **72,** S43–S60.

Boore, D. M., and N. M. Toksöz (1969). Rayleigh wave particle motion and crustal structure, *Bull. Seismol. Soc. Am.* **59,** 331–346.

Bormann, P. (2012). *New Manual of Seismological Observatory Practice (NMSOP-2)*, IASPEI, GFZ German Research Centre for Geosciences, Potsdam, Germany.

Bullen, K. E., and B. A. Bolt (1985). *An Introduction to the Theory of Seismology*, Cambridge University Press, Cambridge, United Kingdom.

Campbell, K. W. (1985). Strong motion attenuation relations: A ten-year perspective, *Earthq. Spectra* **1,** 759–804.
Davis, P., and J. Berger (2007). Calibration of the global seismographic network using tides, *Seismol. Res. Lett.* **78,** no. 4, 454–459, doi: 10.1785/gssrl.78.4.454.
Davis, P., M. Ishii, and G. Masters (2005). An assessment of the accuracy of GSN sensor response information, *Seismol. Res. Lett.* **76,** no. 6, 678–683, doi: 10.1785/gssrl.76.6.678.
Douglas, J. (2001). *A Comprehensive Worldwide Summary of Strong-Motion Attenuation Relationships for Peak Ground Acceleration and Spectral Ordinates (1969 to 2000)*, Imperial College of Science, Technology and Medicine, Civil Engineering Department, London, United Kingdom.
Ekström, G., C. A. Dalton, and M. Nettles (2006). Observations of time-dependent errors in long-period instrument gain at global seismic stations, *Seismol. Res. Lett.* **77,** no. 1, 12–22, doi: 10.1785/gssrl.77.1.12.
Havskov, J., and G. Alguacil (2004). *Instrumentation in Earthquake Seismology*, Springer, Dordrecht, The Netherlands.
Jain, A. K., and R. C. Dubes (1988). *Algorithms for Clustering Data*, Prentice Hall, Englewood Cliffs, New Jersey.
Kanamori, H. (1977). The energy release in great earthquakes, *J. Geophys. Res.* **82,** 2981–2987.
Langston, C. A. (1979). Structure under Mount Rainier, Washington, inferred from teleseismic body waves, *J. Geophys. Res.* **84,** 4749–4762.
MacArthur, A. (1985). Geophone frequency calibration and laser verification, *Geophysics* **50,** 49–55.
MacWilliams, F. J., and N. J. Sloane (1976). Pseudo-random sequences and arrays, *Proc. IEEE* **64,** 1715–1729.
National Geophysical Data Center (2006). *2-Minute Gridded Global Relief Data (ETOPO2) v2*, National Geophysical Data Center, NOAA, doi: 10.7289/V5J1012Q.
Obara, K., K. Kasahara, S. Hori, and Y. Okada (2005). A densely distributed High-Sensitivity Seismograph Network in Japan: Hi-net by National Research Institute for Earth Science and Disaster Prevention, *Rev. Sci. Instrum.* **76,** 021301, doi: 10.1063/1.1854197.
Okada, Y., K. Kasahara, S. Hori, K. Obara, S. Sekiguchi, H. Fujiwara, and A. Yamamoto (2004). Recent progress of seismic observation networks in Japan: Hi-net, F-net, K-NET and KiK-net, *Earth Planets Space* **56,** xv–xxviii.
Park, S., and M. Ishii (2018). Near-surface compressional and shear wave speeds constrained by body-wave polarization analysis, *Geophys. J. Int.* **213,** 1559–1571.
Pavlis, G. L., and F. L. Vernon (1994). Calibration of seismometers using ground noise, *Bull. Seismol. Soc. Am.* **84,** 1243–1255.
Pearson, K. (1901). Principal components analysis, *London Edinburgh Dublin Philos. Mag. J.* **2,** 566.
Silver, P. G., and W. W. Chan (1991). Shear wave splitting and subcontinental mantle deformation, *J. Geophys. Res.* **96,** 16,429–16,454.
Townsend, B. (2014). Symmetric triaxial seismometers, in *Encyclopedia of Earthquake Engineering*, M. Beer, I. Kougioumtzoglou, E. Patelli, and S.-K. Au (Editors), Springer, Berlin/Heidelberg, Germany.
Ueno, T., T. Saito, K. Shiomi, and Y. Haryu (2015). Monitoring the instrument response of the high-sensitivity seismograph network in Japan (Hi-net): Effects of response changes on seismic interferometry analysis, *Earth Planets Space* **67,** no. 1, 135.
Veith, K. F., and G. E. Clawson (1972). Magnitude from short-period P-wave data, *Bull. Seismol. Soc. Am.* **62,** 435–452.
Wessel, P., and W. H. Smith (1991). Free software helps map and display data, *Eos Trans. AGU* **72,** 441–446.
Wielandt, E. (2002). Seismic sensors and their calibration, in *IASPEI–New Manual of Seismological Observatory Practice*, P. Bormann (Editor), GeoForschungsZentrum Potsdam, Potsdam, Germany.

Sunyoung Park[1]
Miaki Ishii
Department of Earth and Planetary Sciences
Harvard University
20 Oxford Street
Cambridge, Massachusetts 02138 U.S.A.
sunnyp@caltech.edu
ishii@eps.harvard.edu

Published Online 27 December 2018

[1] Now at Division of Geological and Planetary Sciences, California Institute of Technology, 1200 E. California Boulevard, Seismological Laboratory 252-21, Pasadena, California 91125 U.S.A.